

*Electronic Supplementary Information (ESI)*

**Electrochemical Interfacing of Prussian Blue Nanocrystals with a Modified Ru Complex Thin-Film on an ITO Electrode**

Hiroaki Sato,<sup>a</sup> Mitsutoshi Ide,<sup>a</sup> Ryo Saito,<sup>a</sup> Takanari Togashi,<sup>b</sup> Katsuhiko Kanaizuka,<sup>b</sup> Masato Kurihara,<sup>b</sup> Hiroshi Nishihara,<sup>c</sup> Hiroaki Ozawa<sup>a</sup> and Masa-aki Haga<sup>\*a</sup>

<sup>a</sup> *Department of Applied Chemistry, Faculty of Science and Engineering, Chuo University, 1-13-27 Kasuga, Bunkyo-ku, Tokyo 112-8551, Japan.*

<sup>b</sup> *Faculty of Science, Yamagata University, 1-4-12 Kojirakawa-machi, Yamagata-shi, 990-8560, Japan.*

<sup>c</sup> *Department of Chemistry, Graduate School of Science, The University of Tokyo, 7-3-1 Hongo, Bunkyo-ku, Tokyo 113-0033, Japan*

**List of Electronic Supporting Information (ESI)**

- 1) Experimental section-** Fabrication of Ru-NP primerlayer on ITO and spontaneous growth of PB crystal films, ITO||(Ru-NP)<sub>3</sub>/PB.
- 2) Figure S1:** Photographs of ITO||(Ru-NP)<sub>3</sub>/PB thin films.
- 3) Figure S2:** SEM image and size distribution of the deposited PB nanocrystals of the Ru-NP modified ITO electrode using two different concentration of Fe<sup>3+</sup> and Fe(CN)<sub>6</sub><sup>3-</sup>.
- 4) Figure S3:** Temporal change of CVs with increasing the film thickness of PB on the Ru-NP-modified ITO electrodes by the increase of the immersion time.
- 5) Table S1.** Peak potentials on CV in ITO||(Ru-NP)<sub>3</sub>/PB thin films: in 0.1 M KCl.
- 6) Table S2.** The change of UV absorption maxima on ITO||(Ru-NP)<sub>3</sub>/PB film
- 7) Figure S4.** Proposed catalytic mechanism for the formation of PB state through the electron transfer mediation of Ru-NP layer.
- 8) Table S3.** Summary of XPS Fe 2p binding energies from the deconvolution of XPS Fe 2p peaks.

## Experimental section

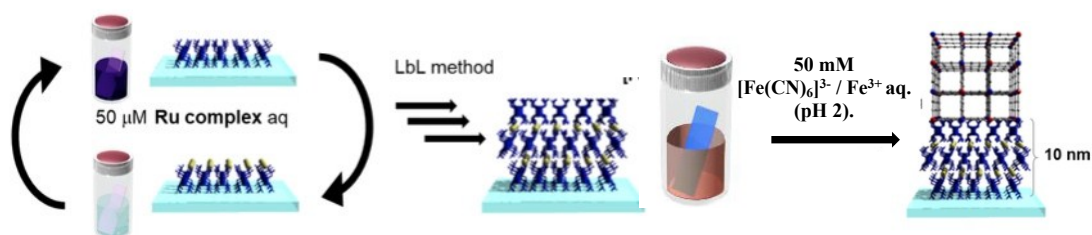
### Fabrication of Ru-NP primerlayer on ITO and spontaneous growth of PB crystal films, ITO||(Ru-NP)<sub>3</sub>/PB.

The complex, **Ru-NP**, was synthesized according to previously published literature procedure. For the modification of an ITO electrode, **Ru-NP** (50  $\mu\text{M}$ ) was dissolved in water by adjusting the pH 6 as an immersing solution. an aqueous solution of  $\text{ZrOCl}_2$  (20 mM), and an indium-tin oxide (ITO) electrode (Kuramoto Co.; surface resistance  $< 10 \Omega\text{cm}^{-1}$ , surface roughness,  $R_a < 0.5 \text{ nm}$ ) were used for the preparation of the films.

An indium-tin oxide (ITO) electrode, purchased from Kuramoto Co. (surface resistance  $< 10 \Omega\text{cm}^{-1}$ , and the surface roughness,  $R_a < 0.5 \text{ nm}$ ) was cleaned by the Radio Corporation of America (RCA) treatment. ITO electrodes were exposed to sonication in a mixture of  $\text{H}_2\text{O}-\text{H}_2\text{O}_2-\text{NH}_4\text{OH}$  (5:5:1, v/v/v) at  $80^\circ\text{C}$  for 1 h, before being washed with copious amounts of ultrapure water and dried under a flow of  $\text{N}_2$ . The pre-cleaned ITO electrode was immersed for 3-6 h in an aqueous solution of the **Ru-NP** (50  $\mu\text{M}$ ), followed by rinsing with copious amounts of ultrapure water and drying under a flow of  $\text{N}_2$ . As a result, ITO||(Ru-NP) was formed, in which the ITO surface was fully covered with the **Ru-NP**. For the fabrication of bi- and trilayer LbL films, the homo-films were grown by successive alternating exposure of the primer layer ITO||(Ru-NP) to an aqueous solution of  $\text{ZrOCl}_2$  (20 mM) for 30 min and then the corresponding **Ru-NP** solutions (3 h) at room temperature in twice and three times. Depending on the number of immersions, homolayer ITO||(Ru-NP)<sub>n</sub> films were formed where the subscript “n” indicates the number of the successive immersing process in the solutions of  $\text{ZrOCl}_2$  and **Ru-NP**.

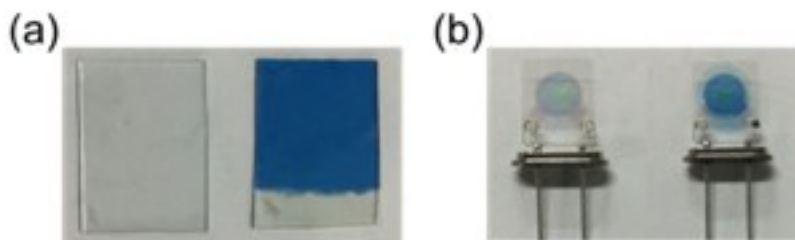
The **Ru-NP** trilayer-modified ITO substrate was immersed in a mixed solution of  $\text{Fe}^{3+}$  and  $[\text{Fe}(\text{CN})_6]^{3-}$  at room temperature ( $\sim 20^\circ\text{C}$ ) in air. A mixed solution of  $\text{Fe}^{3+}$  and  $[\text{Fe}(\text{CN})_6]^{3-}$  was prepared by mixing  $\text{FeCl}_3 \cdot 6\text{H}_2\text{O}$  (50 mM),  $\text{K}_3[\text{Fe}(\text{CN})_6]$  (50 mM), and  $\text{HCl}$  (50 mM) at a 2:2:1 (v/v) ratio. Spontaneous growth of PB crystals on **Ru-NP** primer-layered ITO occurred, and the measurement sample of the ITO||(Ru-NP)<sub>3</sub>/PB nanocrystal film was obtained after 8~12 h immersion.

**Scheme 1.** Protocol for the fabrication of ITO||(Ru-NP)<sub>3</sub>/PB thin films



For the fabrication of EQCM chip modified by ITO||(Ru-NP)<sub>3</sub>/PB nanocrystal, almost the same procedure above was performed except the use of QCM chip holder as a container of the immersing solution.

of the substrates Figure S1.



The photographs modified ITO are shown in

**Figure S1.** □ Photographs of ITO||(Ru-NP)<sub>3</sub>/PB thin films: (a) original ITO (left) and ITO||(Ru-NP)<sub>3</sub>/PB hetero film left in air (right), and (b) EQCM ITO chip (left) and EQCM chip modified by ITO||(Ru-NP)<sub>3</sub>/PB film (right).

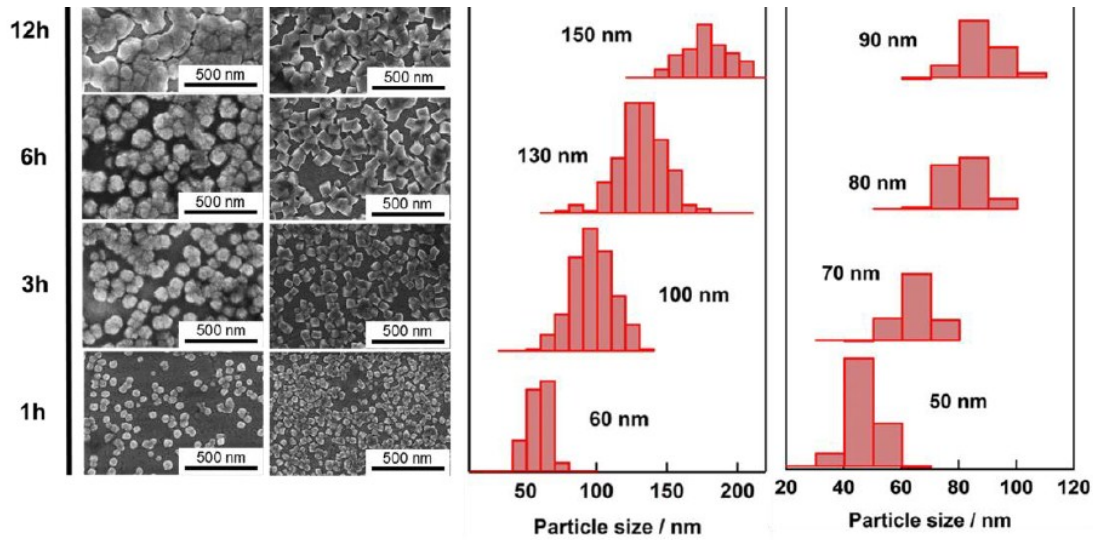


**Figure S2.** SEM image and size distribution of the deposited PB nanocrystals of the Ru-NP modified ITO electrode using two different concentration of Fe<sup>3+</sup> and Fe(CN)<sub>6</sub><sup>3-</sup> (10 mM and 50 mM) by changing immersing time; time interval = 1, 3, 6, and 12 h.

### Dipping time dependence on CV

As the dipping time determines the surface coverage and film thickness of the PB nanocrystals, we investigated the dependence of the CV profiles on the dipping time for different layer numbers ( $n = 1$  and 3). Figure 8a shows the changes in the CV curves with increasing dipping time during the growth of ITO||(Ru-NP)<sub>1</sub>/PB nanocrystals. With increasing immersion time, the peak currents for the two couples of PB gradually increased with the PB crystal growth on the modified ITO surface. Even after 12 h of immersion, the two redox processes for the PW/PB and PB/PY couples were clearly observed, albeit that the peak separation increased (~300 mV). On the other hand, for the growth of PB on the ITO||(Ru-NP)<sub>3</sub> substrate, the changes in the CVs with increasing immersion time were sharper (Figure 8b). After 1 h of immersion, the cathodic peak for the PW/PB couple disappeared and the anodic peak shifted substantially (~200 mV) in anodic direction relative to that of ITO||PB films. When the immersion time was extended beyond 6 h, only the anodic peak from PW to PB and the cathodic peak from PY to PB were observed. These results indicate that ET rectification occurs between the Ru-NP layer and the PB nanocrystal film.

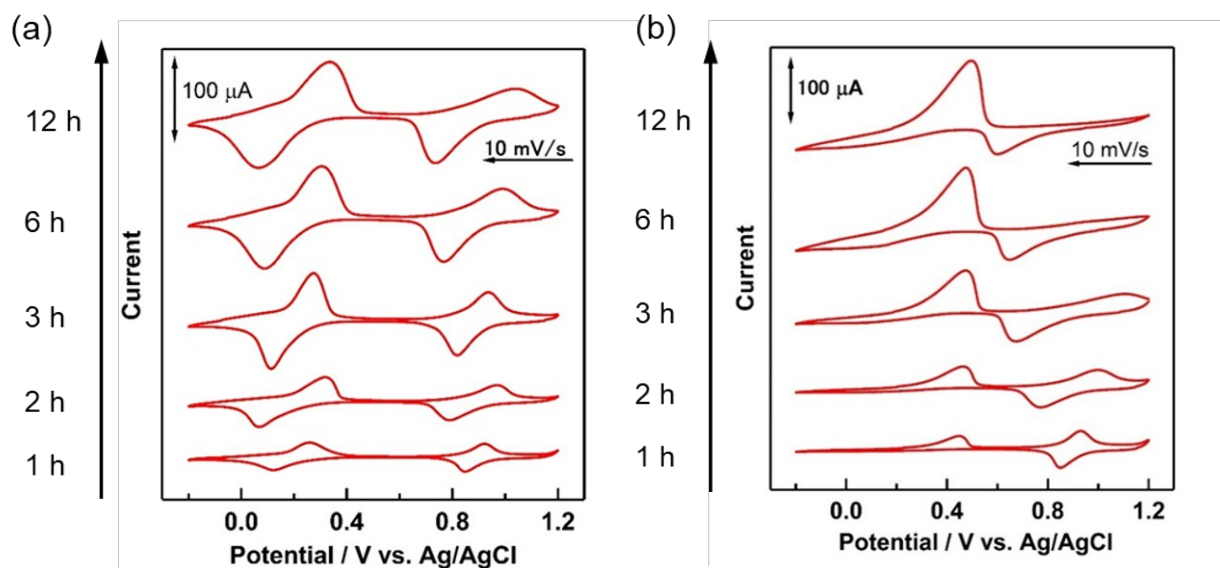


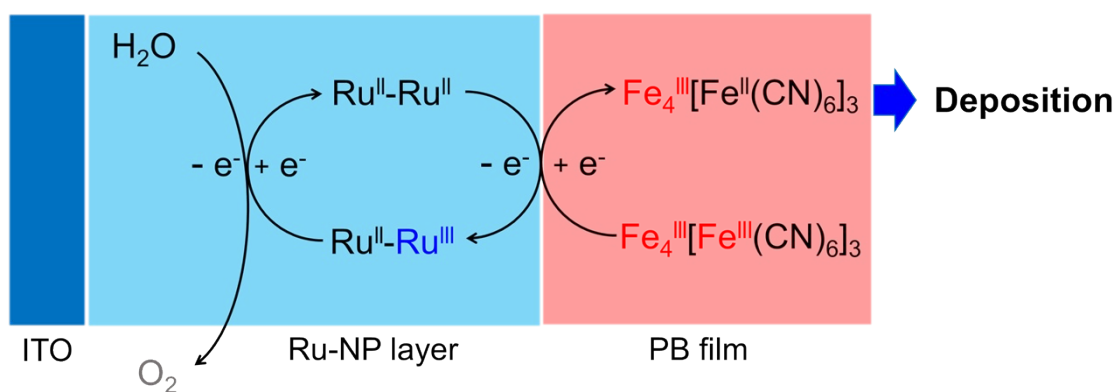
**Figure S3.** CVs of the **Ru-NP**-modified ITO electrodes for increasing PB film thickness with increasing immersion time of the ITO substrate in a mixed solution of  $\text{Fe}^{3+}$  and  $\text{Fe}(\text{CN})_6^{3-}$  (scan rate:  $0.01 \text{ V s}^{-1}$ ; immersion time: 1, 3, 6, 9, and 12 h). The modified ITO substrate was covered with a (a) monolayer or (b) trilayer of **Ru-NP**.

**Table S1.** Peak potentials on CV in ITO||(**Ru-NP**)<sub>3</sub>/PB thin films: in 0.1 M KCl

Number of Ru-NP layer	Immersing time/h	$E^1$ V vs Ag/AgCl		$E^2$	
		$E_{pa}^1$	$E_{pc}^1$	$E_{pa}^2$	$E_{pc}^2$
1	1	0.26	0.13	0.92	0.85
	3	0.32	0.07	0.97	0.79
	6	0.28	0.11	0.94	0.82
	9	0.31	0.09	0.99	0.77
	12	0.34	0.07	1.04	0.73
2	1	0.41	0.02	0.94	0.85
	3	0.44	-	0.98	0.78
	6	0.40	0.07	1.03	0.74
	9	0.44	-0.10	1.14	0.68
	12	0.50	-	-	0.60
3	1	0.45	-	0.93	0.85
	3	0.47	-	1.00	0.77
	6	0.47	-	1.11	0.68
	9	0.47	-	-	0.65
	12	0.48	-	-	0.60

**Table S2.** The change of UV absorption maxima on ITO//(**Ru-NP**)<sub>3</sub>/PB film

Layer	Immersing time / h	$\lambda_{\max}$ / nm (Absorbance)
ITO//( <b>Ru-NP</b> ) <sub>3</sub> /PB	1	710(0.10)
	3	445(0.12), 795(0.43)
	6	433(0.17), 795(0.50)
	12	430(0.24), 825(0.61)

**Figure S4.** Proposed catalytic mechanism for the formation of PB state through the electron transfer mediation of **Ru-NP** layer.

**Table S3.** Summary of XPS Fe 2p binding energies from the deconvolution of XPS Fe 2p peaks<sup>1), 2)</sup>

XPS Fe 2p signals	Binding energy /eV			Assignment of peak <sup>1), 2)</sup>
	Applied potential / V vs Ag/AgCl			
	+1.2 V	+0.6 V	-0.2 V	
Fe 2p <sub>3/2</sub>	709.2	708.8	708.9	Fe(II) low spin
	711.0	712.8	710.4	Fe(III)
	713.7			Fe(III)
		716.0	714.2	Fe(II) satellite
Fe 2p <sub>1/2</sub>	722.1	721.6	721.6	Fe(II)
	724.4	725.3	723.7	Fe(III)
	727.4	727.3	726.3	Fe(III)

### References

- 1) A. Forment-Aliaga, R. T. Weitz, A. S. Sagar, E. J. H. Lee, M. Konuma, M. Burghard and K. Kern, *Small*, 2008, 4, 1671.
- 2) J. Marwan, T. Addou and D. Belanger, *Chem. Mater.*, 2005, 17, 2395.